Halupka, K. J., M. N. Shivdasani, S. L. Cloherty, D. B. Grayden, Y. T. Wong, A. N. Burkitt, and H. Meffin. 2017. Prediction of cortical responses to simultaneous electrical stimulation of the retina. *Journal of Neural Engineering*. **14**(1): 016006.

https://doi.org/10.1088/1741-2560/14/1/016006

Prediction of Cortical Responses to Simultaneous Electrical Stimulation of the Retina

Abbreviated title: Predicting responses to electrical retinal stimulation

Kerry Halupka[1,2,3], Mohit N. Shivdasani[3,4], Shaun L. Cloherty[5,6,1], David B. Grayden[1,3,7], Yan T. Wong[1], Anthony N. Burkitt[1,3,7], Hamish Meffin[5,6]

[1]NeuroEngineering Laboratory, Dept. of Electrical & Electronic Engineering, The University of Melbourne, VIC 3010, Australia.
[2]National ICT Australia, Victoria Research Lab, The University of Melbourne, VIC 3010
[3]Bionics Institute, 384-388 Albert St, East Melbourne, VIC 3002, Australia.
[4]Dept. of Medical Bionics, The University of Melbourne, VIC 3010, Australia.
[5]National Vision Research Institute, Australian College of Optometry, Carlton, VIC 3053, Australia.
[6] Australian Research Council Centre of Excellence for Integrative Brain Function, Department of Optometry and Vision Sciences, The University of Melbourne, Melbourne, VIC 3010, Australia.
[7]Centre for Neural Engineering, The University of Melbourne, VIC 3010, Australia.

Correspondence should be addressed to:
Kerry Halupka
Tel: +61 437 911 079
E-mail: Kerry.halupka@gmail.com
Address:
NeuroEngineering Laboratory
Dept. of Electrical & Electronic Engineering
The University of Melbourne
VIC 3010
Australia.

Page Count	43
Figures	10
Tables	0
Multimedia/3D models	0

Word counts

Abstract	263
Introduction	602
Discussion/Conclusion	2106
Total (Abstract, Intro, Methods, Results, Discussion, Conclusion, Acknowledgements)	**7400**

Predicting responses to electrical retinal stimulation

Abstract

Objective

Simultaneous electrical stimulation of multiple electrodes has shown promise in diversifying the responses that can be elicited by retinal prostheses compared to interleaved single electrode stimulation. However, the effects of interactions between electrodes are not well understood and clinical trials with simultaneous stimulation have produced inconsistent results. We investigated the effects of multiple electrode stimulation of the retina by developing a model of cortical responses to retinal stimulation.

Approach

Electrical stimuli consisting of temporally sparse, biphasic current pulses, with amplitudes sampled from a bi-dimensional Gaussian distribution, were simultaneously delivered to the retina across a 42-channel electrode array implanted in the suprachoroidal space of anesthetized cats. Visual cortex activity was recorded using penetrating microelectrode arrays. These data were used to identify a linear-nonlinear model of cortical responses to retinal stimulation. The ability of the model to generalize was tested by predicting responses to non-white patterned stimuli.

Main results

The model accurately predicted two cortical activity measures: multi-unit neural responses and evoked potential responses to white noise stimuli. The model also provides information about electrical receptive fields, including the relative effects of

each stimulating electrode on every recording site.

Significance

We have demonstrated a simple model that accurately describes cortical responses to simultaneous stimulation of a suprachoroidal retinal prosthesis. Overall, our results demonstrate that cortical responses to simultaneous multi-electrode stimulation of the retina are repeatable and predictable, and that interactions between electrodes during simultaneous stimulation are predominantly linear. The model shows promise for determining optimal stimulation paradigms for exploiting interactions between electrodes to shape neural activity, thereby improving outcomes for patients with retinal prostheses.

Introduction

Retinal prostheses produce phosphenes by electrically stimulating surviving retinal neurons in patients with severe photoreceptor degeneration. Clinical trials have shown that retinal prostheses elicit useful perceptions, resulting in improvements in spatio-motor tasks (Barry et al., 2012; Kotecha et al., 2014; Stingl et al., 2015) and reading (da Cruz et al., 2013). However, spatial resolution with present devices is severely limited with the highest reported visual acuity achieved of 20/546 (Stingl et al., 2013).

One strategy that shows promise to improve resolution is simultaneous stimulation of multiple electrodes. Interactions that occur when combinations of electrodes are stimulated simultaneously are capable of increasing the repertoire of visual percepts that can be elicited compared to conventional single-electrode stimulation. Simultaneous stimulation can activate groups of cells between electrodes (Dumm et al., 2014), reduce current spread by using one or more local return electrodes (Cicione et al., 2012; Habib et al., 2013; Matteucci et al., 2013), and elicit responses at the level of a single cell *in vitro* (Jepson et al., 2014). Clinically, studies have mainly aimed to elucidate perceptual differences between sequential and simultaneous stimulation (Humayun et al., 1999; Rizzo et al., 2003; Auner et al., 2008; Horsager et al., 2010; Wilke et al., 2011). Although these studies were limited to stimulation of electrodes in simple geometric patterns such as lines and squares with identical biphasic pulses on all electrodes, inconsistencies were reported regarding percept predictability and reproducibility.

It is clear that simultaneous stimulation is a promising strategy for eliciting useful

percepts. However, the crucial next step in either reducing or harnessing electrode interactions is to investigate the predictability and reproducibility of responses to simultaneous stimulation, and gain a better understanding of how electrode interactions affect neural responses.

Here, we combine simultaneous stimulation of 42 suprachoroidal electrodes with multi-site recordings in the cat visual cortex, to demonstrate that electrode interactions at the level of the cortex are predominantly linear. Additionally, we show that a simple model comprised of a linear filter followed by a static nonlinearity (hereafter, linear-nonlinear model) can reliably predict neural spiking responses to several different simultaneous stimulation paradigms. We also demonstrate the ability of the same model to predict responses based on an alternative metric of cortical activity, namely, the power in the evoked responses. The predictive success of our model shows promise for efficiently determining optimal stimulation paradigms for shaping neural activity with a retinal prosthesis.

Methods

Experiments were performed in eight normally-sighted, adult cats. All procedures were approved by the Bionics Institute Animal Research Ethics Committee (Projects 12/255AB and 14/304AB).

Anesthesia and Surgery

Cats were anesthetized with an initial dose of ketamine (intramuscular, 20 mg/kg) and xylazil (subcutaneous, 2 mg/kg). Anesthesia was maintained with an intravenous infusion of sodium pentobarbitone (60mg/kg/hr) and Hartmanns solution (sodium lactate, 2.5 mL/kg/hour).Dexamethasone (intramuscular, 0.1 mg/kg) and Clavulox (subcutaneous, 10 mg/kg) injections were given daily to minimize brain swelling and infection. Vitals were continuously monitored throughout the experiment.

Details of the surgical implantation of the suprachoroidal array have been described previously (Shivdasani et al., 2012). Briefly, a lateral incision through the sclera was performed to expose the choroid. The electrode array was then inserted into the suprachoroidal space via a pocket created between the sclera and choroid, and sutured into place (Villalobos et al., 2012).

The suprachoroidal array (Figure 1(a)) consisted of a flexible medical grade silicone substrate with 7 rows x 3 columns of platinum electrodes used in six experiments, and 7 rows x 6 columns of electrodes used in the remaining two experiments. Electrodes were 600 µm in diameter arranged hexagonally with 1 mm

Predicting responses to electrical retinal stimulation

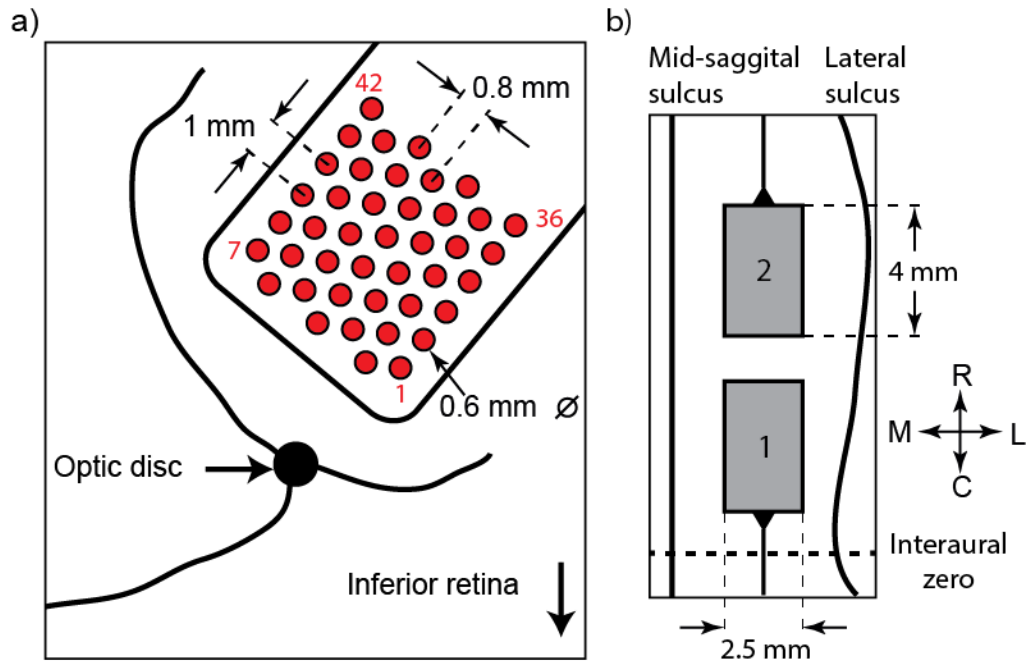

Figure 1. a) Schematic of stimulating array position and dimensions in relation to optic disc; electrode numbering for the four corner electrodes of the array are shown in red. **a)** Schematic of the recording array placements in the hemisphere of the visual cortex contralateral to the implanted eye. R: rostral, C: caudal, M: medial, L: lateral.

center-to-center spacing (Villalobos et al., 2012).

The visual cortex contralateral to the implanted eye was exposed and penetrating microelectrode arrays (either 6 x 10 or 6 x 6 channels, 1 mm length, 400 µm spacing, Blackrock Micro., USA) were implanted Figure 1(b)). Evoked potentials (EPs) from the cortical surface in response to retinal stimulation were used to optimize the position of the implanted arrays (Cicione et al., 2012; Dumm et al., 2014). Neural signals were sampled at 30 kHz (Cerebus Neural Processing System, Blackrock Microsystems, Salt Lake City, UT).

White Noise Stimuli

Temporally sparse electrical pulses delivered simultaneously across the stimulating electrodes were used to characterize the system while responses were recorded in the visual cortex. The stimulus amplitude for each electrode was sampled from a bi-dimensional Gaussian distribution (hereafter, spatially white stimuli). To balance the effect of each electrode on cortical activation, the standard deviation of each Gaussian distribution was the activation threshold for that electrode.

Thresholds were acquired by stimulating each electrode individually with cathodic-first biphasic current pulses using a 1 ms phase width, 25 µs interphase gap, at a 1 Hz presentation rate (the same pulse waveform was used for all electrical stimulation paradigms), and 0-750 µA stimulus amplitude, in 50 µA steps. A spike-rate (or power) versus stimulus amplitude input-output function for each stimulating electrode-recording channel combination was generated to which a sigmoid curve was fitted. For each sigmoid, the stimulus amplitude at 50% of the maximum response was defined as the threshold for that recording channel (Shivdasani et al., 2012). The threshold for each stimulating electrode was chosen to be the lowest threshold over all recording channels for which a sigmoid could be fit. All electrodes across the array were then stimulated simultaneously with charge-balanced waveforms using a mix of anodic and cathodic-first polarities with current amplitudes determined by the stimulus matrix. There were 3600 white-noise stimulation patterns generated for each experiment; these were presented eight times, with the average of the responses on each recording channel used for analysis.

To investigate variability in cortical responses to repeated white noise stimuli, 60 repetitions of 30 different white noise patterns were presented in a randomized order in

three of the experiments. The mean and standard deviation of the responses to each of these patterns was calculated.

Oriented Pattern Stimuli

Stationary, oriented electrical stimulus patterns were presented to test the prediction ability of the model with non-white stimuli. These patterns were electrical representations of sinusoidal gratings at six possible orientations (0, 30, 60, 90, 120, and 150 degrees), five spatial frequencies (ranging over approximately 1-3 cycles per array length), and scaled by five stimulating currents (i.e., amplitudes of stimulating currents on each electrode were scaled by 175, 235, 295, 355, or 415 μA). Patterns consisted of three main types: (i) mixed-phase first stimuli (Figure 2(a)), where some electrodes on the array were stimulated with anodic-phase first biphasic pulses while others were stimulated with cathodic-phase first biphasic pulses; (ii) anodic-phase first stimuli (Figure 2(b)), where all electrodes on the array were stimulated with anodic-phase first biphasic pulses; (iii) cathodic-phase first stimuli (Figure 2(c)), where all electrodes on the array were stimulated with cathodic-phase first biphasic pulses. During each experiment, 30 different pattern stimuli were presented in a randomized order, with 10 repetitions of each pattern stimulus.

Data Pre-Processing

Two measures were used to estimate the cortical activity: power in the evoked potential (EP power) that occurred within approximately 20 ms of the stimulus pulse and multi-unit activity (MUA) in the same time frame.

Predicting responses to electrical retinal stimulation

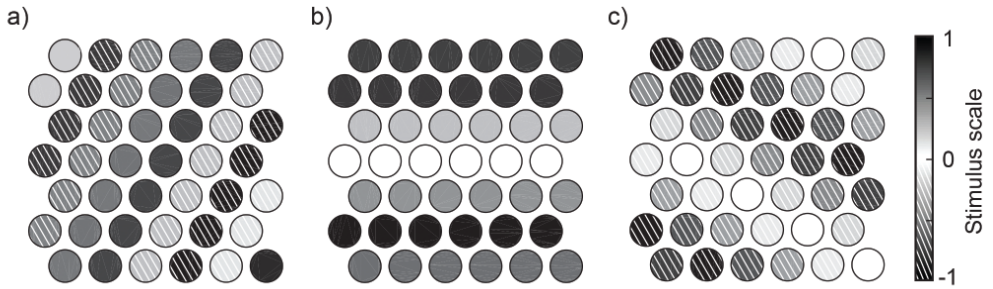

Figure 2. Example electrical stimulation patterns used as oriented electrical stimuli. The weighting of each electrode is represented by a grayscale, with black being the strongest weighting on the array (and thus the biggest current amplitude). White represents zero current amplitude. Electrodes with cathodic-phase first stimuli are hatched in white. **a)** Mixed-phase stimulus. **b)** Anodic-phase first only stimuli. **c)** Cathodic-phase first only stimuli.

To estimate the power in the evoked responses, offline multi-taper spectral analysis (Thomson, 1982; Mitra and Pesaran, 1999) was used to filter the raw data (400-1400 Hz, 2 tapers, taper length of 4 ms). The log power was then calculated from 3 ms after the end of the stimulus pulse (to exclude the stimulus artifact) until 20 ms after the pulse with the power in the same band in the 500 ms prior to each stimulus subtracted to exclude spontaneous activity.

For the MUA analyses, stimulus artefacts were first removed (Heffer and Fallon, 2008; Cicione et al., 2012; Shivdasani et al., 2012). Following band-pass filtering using a third-order Butterworth filter (300-5000 Hz), multiunit spikes were detected as threshold crossings using a threshold of 4x root-mean-square that was calculated within a 60 s moving time window. Typically, MUA occurred 3-20 ms post-stimulus; however, in some instances, another burst of spikes followed at approximately 30 ms post-stimulus. Only the early component of spiking was analyzed as this is considered to be a result of direct stimulation of retinal ganglion cells (RGCs) and indirect activation of the inner retina, but

not activation of the photoreceptors (Boinagrov et al., 2014). The spontaneous spiking rate on each channel in the 500 ms prior to each stimulus was subtracted to account for variation in the stimulus-independent activity. For both measures, responses on each channel were normalized by the maximum response recorded on the array to any presented stimulus.

Linear-Nonlinear (LN) Model

We developed a model to explain activity in the visual cortex in response to simultaneous multi-electrode stimulation of the retina. Cortical responses to spatially white electrical stimulation of the retina were used to characterize the model. The model consisted of two parallel spatial linear filters that provided estimates of the spatial tuning properties of each cortical recording channel, followed by two parallel static nonlinearities that accounted for nonlinear characteristics of neurons such as response thresholds and saturation.

This model is similar to well-established Gaussian white noise models developed to describe light responses in the retina (Chichilnisky, 2001; Pillow et al., 2005; Schwartz and Rieke, 2011) and RGC responses to simultaneous stimulation of the retina (Maturana et al., 2016). However, several key adaptions have been made to the established model to accommodate the different stimulation method (i.e. electrical vs light stimulation). First, as opposite phase pulses produce a differential response (Jensen and Rizzo, 2006), the effects of both anodic-first and cathodic-first biphasic pulses were included separately in the model. Specifically, two different linear filters ($\boldsymbol{V_P}$ for net anodic-first and $\boldsymbol{V_N}$ for net cathodic-first stimuli) and their associated static nonlinearities (g_P and g_N) acted on the input ($\boldsymbol{S}$) separately (Figure 3).

Predicting responses to electrical retinal stimulation

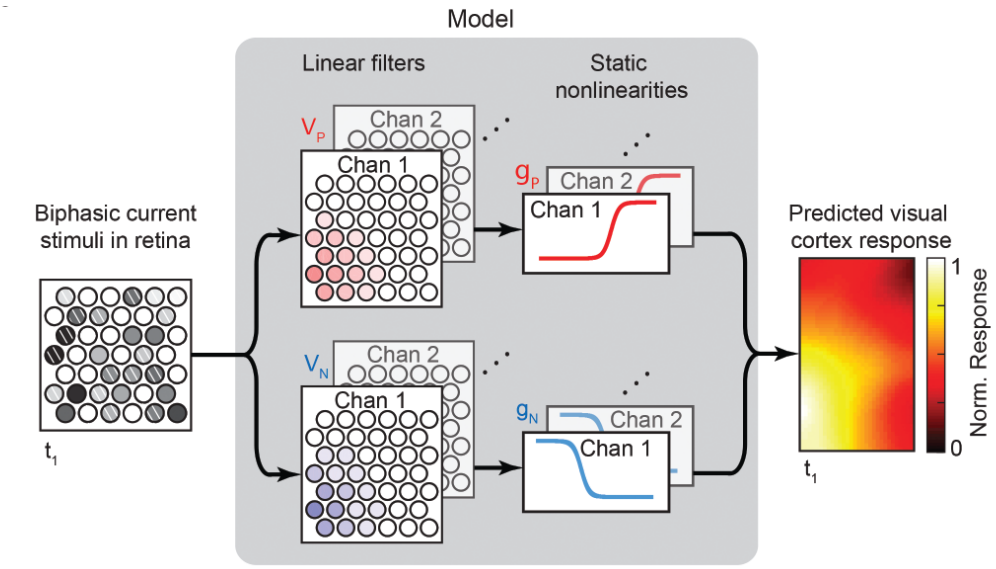

Figure 3. The linear non-linear cascade model of the pathway illustrated between the retina and visual cortex. Shown here is the input signal, arranged in the form of multiple electrode stimulation of the suprachoroidal array. The input is split by the model into a "positive" and a "negative" path, each representing the cortical response to net anodic first and net cathodic first stimuli respectively. After the linear and the nonlinear filters act on either side, the outputs are summed. The summed output is the predicted cortical response to a particular input stimulus. A total of 3600 white noise patterns were presented to the retina, here t_1 refers to a single stimulus and its resulting predicted response.

Our model also accommodated the larger range of response amplitudes present in our data and adjusted to describe response amplitude, rather than spike probability. Additionally, we recorded cortical responses at multiple sites (up to 120) concurrently during stimulation and, as such, a LN model was fitted independently for each channel; thus, the index for each channel is omitted from the equations below for clarity.

An estimate of the activity (spike count or EP power) at each time t ($t \in \{1 \dots T\}$),

at a given site in the cortex, is given by

$$\boldsymbol{R}_{\text{est}} = g_P(\boldsymbol{S}^T\boldsymbol{V}_P) + g_N(\boldsymbol{S}^T\boldsymbol{V}_N). \quad (1)$$

Each column of the stimulus matrix $\boldsymbol{S}$ contains the stimulation amplitude applied at time t with a row for each stimulating electrode j ($j \in \{1 \dots M\}$), where T is the number of stimuli that resulted in a response; the stimulus vector at time t is thus given by

$$\boldsymbol{s_t} = \begin{pmatrix} s_{1,t} \\ \vdots \\ s_{M,t} \end{pmatrix}. \quad (2)$$

The normalized stimulus vector is thus given by

$$\bar{\boldsymbol{s}}_t = \begin{pmatrix} s_{1,t}/\sigma_1 \\ \vdots \\ s_{M,t}/\sigma_M \end{pmatrix}. \quad (3)$$

where σ_M is the activation threshold of each stimulating electrode. Since more than one spike was sometimes recorded per stimulus, the spike triggered covariance is given by

$$\boldsymbol{C}_{\text{STC}} = \frac{1}{N}\sum_{t=1}^{T} r_{i,t}\bar{\boldsymbol{s}}_t\bar{\boldsymbol{s}}_t^{\boldsymbol{T}}. \quad (4)$$

where $r_{i,t}$ is the response on recording channel i ($\{i \in 1 \dots C\}$), at time t, and N is the sum of responses on that channel.

The combined effect of all stimulating electrodes on a response in a given cortical channel could be either net anodic-first or net cathodic-first. Therefore, the effects of both anodic-first and cathodic-first biphasic pulses were included separately in the model. Responses due to a net anodic-first stimulation ($\boldsymbol{R}_P$) were those where the projections of

the stimulus onto the principal eigenvector of $\boldsymbol{C_{STC}}$ (denoted $\boldsymbol{u_{STC}}$) were positive. Stimuli for which this held true were denoted $\bar{\boldsymbol{s}}_P$, such that

$$\bar{\boldsymbol{s}}_P \cdot \boldsymbol{u}_{\mathrm{STC}} > \mathbf{0}. \tag{5}$$

Responses to a net cathodic-first stimulation ($\boldsymbol{R}_N$) were those for which the projections onto the principal eigenvector were negative,

$$\bar{\boldsymbol{s}}_N \cdot \boldsymbol{u}_{\mathrm{STC}} < \mathbf{0}, \tag{6}$$

where $\bar{\boldsymbol{s}}_N$ were the corresponding cathodic-first stimuli.

The linear filter estimates $\boldsymbol{V}_{P,\mathrm{est}}$ and $\boldsymbol{V}_{N,\mathrm{est}}$ were then calculated as the spike triggered average (Chichilnisky, 2001) of response subsets $\boldsymbol{r}_P$ and $\boldsymbol{r}_N$ and their respective stimuli ($\boldsymbol{s}_P$ and $\boldsymbol{s}_N$),

$$\boldsymbol{V}_{P,\mathrm{est}} = \frac{\boldsymbol{r_P^T}\bar{\boldsymbol{s}}_{\boldsymbol{P}}}{N_P} \tag{7}$$

and

$$\boldsymbol{V}_{N,\mathrm{est}} = \frac{\boldsymbol{r_N^T}\bar{\boldsymbol{s}}_{\boldsymbol{N}}}{N_N}, \tag{8}$$

where N_P and N_N are the sum of response subsets $\boldsymbol{r_P}$ and $\boldsymbol{r_N}$, respectively, such that $N_P + N_N = N$. Filters were then normalized by dividing by their L-2 norm. These $\boldsymbol{V}_{P,\mathrm{est}}$ and $\boldsymbol{V}_{N,\mathrm{est}}$ vectors were considered to be weightings for the effect of the stimulating electrodes on a given cortical site.

The static nonlinearities g_P and g_N were approximated by sigmoids and parameterized by their saturation amplitudes (y_P and y_N), thresholds (a_P and a_N) which are 50% of the saturation level, as well as the gain of the sigmoids (b_P and b_N). The equations for the static nonlinearities g_P and g_N are

$$g_P(r) = \frac{y_P}{1 + e^{(-b_P(x_P - a_P))}} \quad (9)$$

$$g_N(r) = y_N - \frac{y_N}{1 + e^{(-b_N(x_N - a_N))}}. \quad (10)$$

We used the distribution of the outputs of the linear filters, $x_P = \bar{\boldsymbol{s}}_{\boldsymbol{P}}\boldsymbol{V}_{P,\mathrm{est}}$ and $x_N = \bar{\boldsymbol{s}}_{\boldsymbol{N}}\boldsymbol{V}_{N,\mathrm{est}}$ (hereafter referred to as generator signals), and corresponding responses $\boldsymbol{r_P}$ and $\boldsymbol{r_N}$, to provide an initial estimate for the parameters of non-linear functions g_P and g_N respectively. The threshold values a_{P} and a_{N} were estimated to be the mean values of their respective generator signals, while y_P and y_N were estimated as that maximum average response recorded on any channel (averaged over repeated trials). We used a Levenberg-Marquardt non-linear least squares algorithm in MATLAB (Mathworks, Inc. USA) to find the optimal non-linear parameters (a_{P}, a_{N}, b_P, b_N, y_P and y_N) and confirm that the optimal linear filters were $\boldsymbol{V}_{P,\mathrm{est}}$ and $\boldsymbol{V}_{N,\mathrm{est}}$. The outcome of this process was a set of linear filters and static nonlinearities, each corresponding to a different recording channel (shown for one recording channel in Figure 5).

To test which electrodes significantly affected a recording channel's response, we randomly time-shifted the response vector 1000 times and repeated the above analysis (Equations 1-8) for each new response subset. This generated a distribution for $\boldsymbol{V}_{P,\mathrm{est}}$ and $\boldsymbol{V}_{N,\mathrm{est}}$ to which the true vectors could be compared. Electrodes from the true $\boldsymbol{V}_{P,\mathrm{est}}$ and $\boldsymbol{V}_{N,\mathrm{est}}$ that were larger than the root mean square of the randomly-generated distribution were considered significant. The spatial extent in the retina over which a cortical site is influenced by is given by:

$$D_P = \frac{\sum_{j=1}^{M} v_j^P d_j}{v_j^P} \quad (11)$$

$$D_N = \frac{\sum_{j=1}^{M} v_j^N d_j}{v_j^N}, \quad (12)$$

where d_j is the distance of each electrode j to the center of mass of the significant electrodes, and v_j^P and v_j^N are the weights given by $\boldsymbol{V}_{P,\mathrm{est}}$ and $\boldsymbol{V}_{N,\mathrm{est}}$, respectively.

Statistical Analysis

To compare the sizes of $\boldsymbol{V}_{P,\mathrm{est}}$ and $\boldsymbol{V}_{N,\mathrm{est}}$, we conducted a sign test to determine whether the results of subtracting the filters for each channel were significantly different to zero. False Discovery Rate correction (Benjamini and Hochberg, 1995) was used to control for multiple comparisons to a level of $p < 0.05$. We used the same analysis to compare the sizes of $\boldsymbol{V}_{P,\mathrm{est}}$ and $\boldsymbol{V}_{N,\mathrm{est}}$ between the two model types (MUA model and EP power model).

To demonstrate the ability of the model to predict cortical responses to spatially white electrical retinal stimulation, we performed a 6-fold cross validation analysis on all eight experiments for models fitted to both MUA and evoked response power. For this, the model was fitted using only 5/6 of the white noise data and used to predict the remaining 1/6 of the data. Only recording sites that exhibited a monotonic increase of activity with current in response to single electrode stimulation of at least one stimulating electrode were included in model fitting and analysis. Cross-correlation analyses were performed to compare the predicted and recorded responses. The coefficient of determination and slope of the line of best fit (where the predicted response was the independent variable) were calculated for each of the cross-validation sets independently. Unless otherwise stated, all figures with error bars show the mean and standard error of the mean. Significant differences between the prediction abilities of the model fitted to MUA versus

that fitted to evoked response power were tested using a Wilcoxon Rank sum test ($p < 0.05$).

In order to rule out any correlations due to chance, we estimated the number of responses to white noise patterns in the trial set that could be accurately predicted by the model. A bootstrap test was performed (10,000 samples) comparing the absolute residual error of prediction for each white noise pattern in the trial set against a distribution composed of the absolute residual error of recorded responses versus time-shifted predictions, over all fitted channels. False Discovery Rate correction (Benjamini and Hochberg, 1995) was used to control for multiple comparisons to a level of $p < 0.05$.

We then tested the ability of a model trained with responses to white-noise stimuli to predict responses to the oriented pattern stimuli. Models used in these predictions were fitted to all of the responses to white-noise stimuli (rather than just 5/6 of the data). Here, the coefficient of determination and slope of the line of best fit was calculated for each of the five stimulation amplitudes separately for all eight experiments. Further bootstrap analyses similar to those performed with the white noise data were also performed on the pattern stimuli data to rule out any correlations that may have occurred due to chance. The same analysis was performed to compare the predicted and measured responses to single electrode stimulation, using the data obtained to calculate single electrode thresholds. In addition to comparing the absolute residual error to the bootstrapped distribution, the coefficient of determination between the predicted and recorded responses to above-threshold single electrode stimulation was also compared in the same manner.

Results

Across eight experiments, visual cortex responses to multi-electrode stimulation of the retina were recorded and analyzed in the form of MUA and EP power on a total of 696 recording channels.

Cortical Responses to Multi-Electrode Suprachoroidal Stimulation

Figures 4(a) and 4(b) show raw recording traces from two recording sites following a stimulus pulse, indicating evoked responses, and the presence of spiking activity, respectively (to a white noise stimulus). Evoked responses typically consisted of two prominent peaks occurring a few milliseconds apart (Fig. 4(a)), sometimes followed by a third peak, resulting in a significant increase in power from the baseline response (Fig. 4(e)). Both response measures exhibited a characteristic, monotonically increasing sigmoidal relationship with current amplitude (Figure 4(c,d)) (Cicione et al., 2012; Shivdasani et al., 2012; Dumm et al., 2014). However, significantly more channels exhibited this effect for EP power than MUA (MUA vs. EP power: 66.6% ± 6.1 vs. 92.4% ± 3.2, p = 0.0029; Rank sum test; N=8).

Predicting responses to electrical retinal stimulation

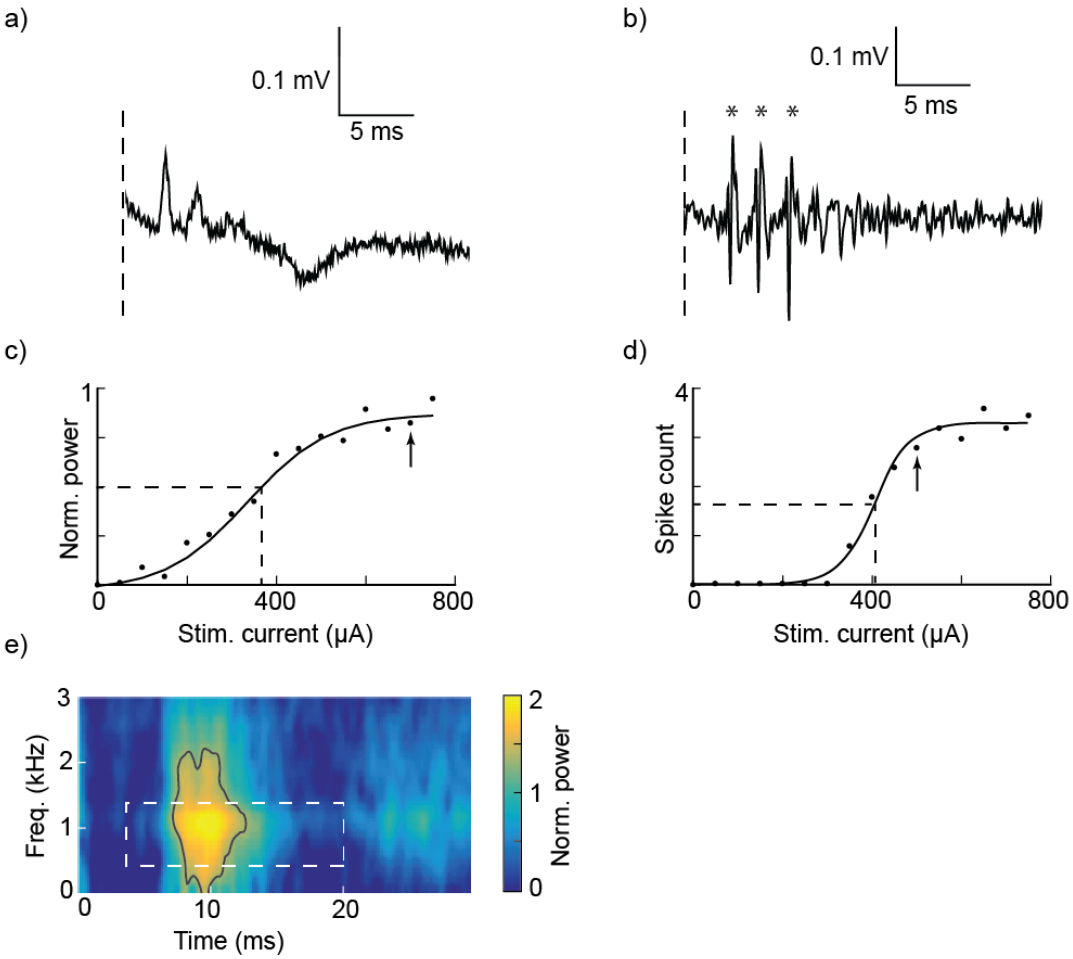

Figure 4. a) Raw response on one recording channel from a single electrode stimulus at 700 μA, showing a multi-peaked evoked potential; dashed line shows the end of the stimulus artefact. **b)** Filtered trace on a different recording channel, showing spiking (indicated by asterisks) in response to single electrode stimulation. **c, d)** Transfer functions of the power in the multi-peaked evoked potential (c) and spike count (d) versus stimulation amplitude, with a sigmoidal line of best fit. Dashed lines show the thresholds of these particular stimulating electrodes at 50% of maximum response. The arrows show the average normalized power and spike count for responses shown in panels a and b respectively. **e)** Power spectrum of the multi-peaked response shown in panel a. The black outline indicates significant increase in power from the baseline response. White dashed box indicates the time and frequency window within which the EP power is calculated.

Prediction of Cortical Responses

Models for the response on each channel were fitted independently, and parametrized by two linear filters and two static nonlinearities (Figure 5). The linear filters derived analytically (Equations 2-8) and the optimized linear filters were compared, showing that the filters were largely identical before and after optimization, with a median r^2 correlation coefficient of 0.93. The optimized linear filters and nonlinearity parameters were used in all further analyses. Figure 5 shows the components of the model for one recording channel. As shown by the linear filters, which can be considered to be the electrical receptive fields (ERFs) for each cortical channel, this particular recording site was maximally activated by pulses on the top left edge of the stimulating array. The static nonlinearities are functions of the action of the linear filters on the stimulus vector. For this recording channel, the model prediction of the responses (Figure 5(c)) was in close agreement with the recorded responses shown in grey (mean ± SEM of the binned responses) (coefficient of determination r^2=0.865).

Predicting responses to electrical retinal stimulation

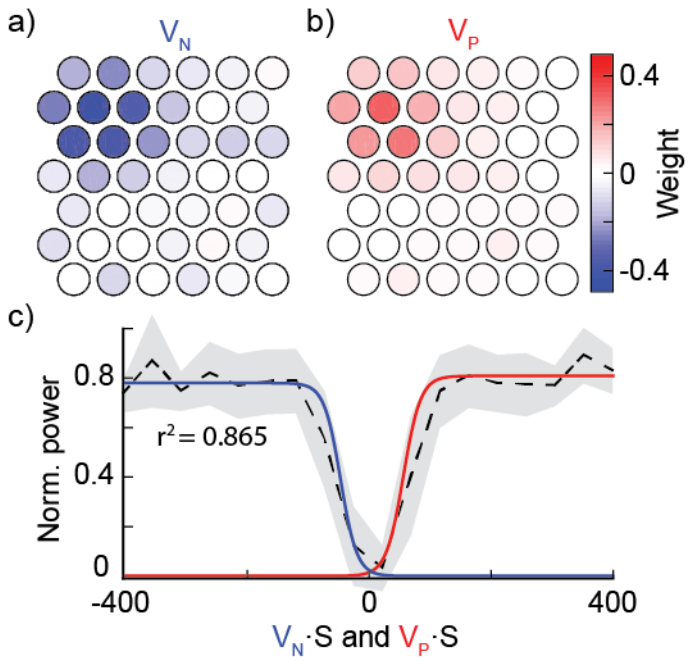

Figure 5. Model components for a single recording channel, as shown schematically in Figure 3, fitted with EP power in response to 5/6th of the white noise stimuli in one experiment. **a)** Spatial linear filters V_N and **b)** V_P, where each circle represents a stimulating electrode on the retinal array, and color refers to the strength of the linear filter. **c)** Static nonlinearities g_N (blue line) and g_P (red line). The y axis is normalized to the maximum average EP power recorded on any channel. Dashed black line shows the average recorded response to each of the binned generator signal levels (mean ± SEM, shown in grey) (r^2=0.865).

Validating Model Fit

For the averaged responses to stimuli to be a reasonable metric to fit the model, the stimulus response variability must be minimal. Figure 6(a) shows the measured EP power (mean ± SE) for all recording channels in response to 60 repetitions of a white noise stimulus pattern in one experiment. Only minor variation in responses was observed, and a clear and significant correlation was seen with the responses predicted

Predicting responses to electrical retinal stimulation

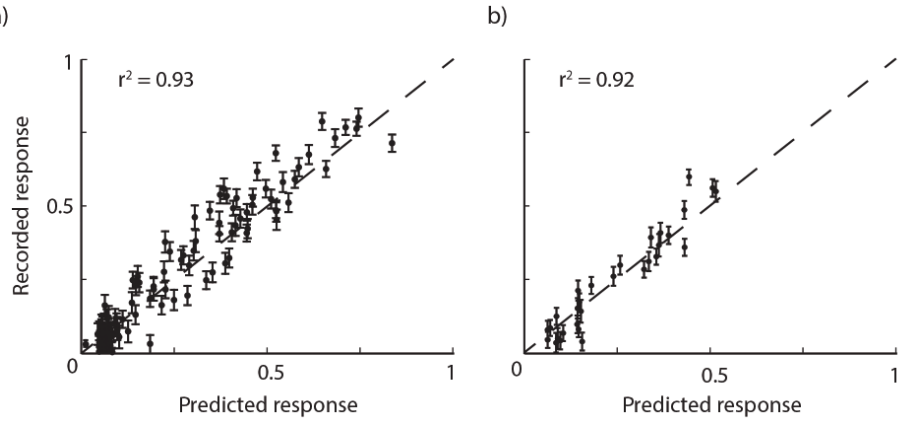

Figure 6. Mean and standard error of recorded responses (n=60 repetitions of each stimulus) plotted against the responses predicted by the model. Response measure is power in the multi-peaked EP. a) Responses on 88 cortical channels in one experiment to 60 repetitions of a single white noise stimulus. b) Responses on a single recording channel in the same experiment as in panel a, to 60 repetitions of 30 separate white noise stimuli.

by the model (r^2 = 0.93, p<0.0001, FDR corrected permutation test, 10 million permutations). The same metric, but for a single cortical channel in response to 30 different white noise stimuli each repeated 60 times, is shown in Figure 6(b). Again, only minor variation in response was observed, with a clear and significant correlation (r^2 = 0.92, p<0.0001, FDR corrected permutation test, 10 million permutations).

The stimuli used to fit the model comprised 3600 different white noise patterns, averaged over eight repeats. For one such white noise stimulus (Figure 7(a)), a comparison of the recorded and predicted responses (Figure 7(b)) indicates that the model prediction of the response was very similar to the measured response, which was borne out by a coefficient of determination of r^2=0.936 (Figure 7(c)), with a strong overall correlation observed for this experiment (r^2=0.819, Figure 7(d)).

Predicting responses to electrical retinal stimulation

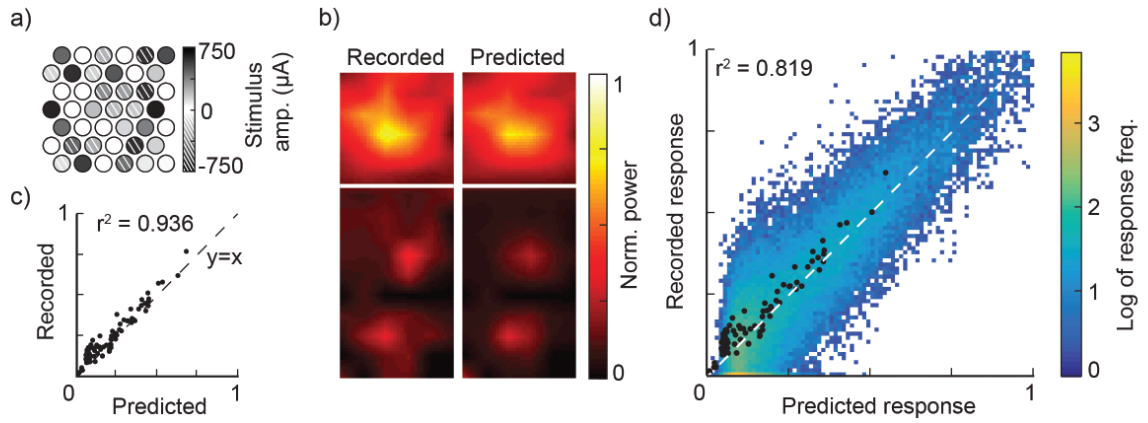

Figure 7. a) Example of a white-noise stimulus in one experiment with positive currents indicating anodic-first pulses and negative currents indicating cathodic-first pulses. **b)** Recorded and predicted EP power in the visual cortex across two recording arrays in response to the white noise stimulus shown in panel a (averaged over 8 repetitions). **c)** Correlation between the recorded response to the stimulus and the response predicted by the model. Each point represents the response measured on a single recording channel. Dashed line is y=x. **d)** Aggregated scatter plot for all 600 white-noise stimuli that were not used to fit the model for this experiment, with the log frequency of responses represented on the color scale. Black dots show the responses presented in panel c.

Similar correlations were found for all six cross-validated models for all eight experiments, with $0.55<r^2<0.89$ (n=48). Models fitted to MUA displayed significantly higher correlation coefficients (MUA vs. EP power: $r^2 = 0.77 \pm 0.01$ vs. 0.69 ± 0.02, $p=1.22\times10^{-4}$; Rank sum test) than those fitted to EP power. The average slope of the line of best fit for the models fitted to power was significantly closer to 1 (MUA vs. EP Power: 0.88 ± 0.018 vs. 0.92 ± 0.13, $p=2.13\times10^{-4}$; Rank sum test) than those fitted to MUA.

Both types of models were able to predict the responses to at least 75% of the test set significantly better than chance (via bootstrap analysis), with the MUA model

predicting significantly more than the EP power model (MUA vs. EP Power: 95.77% ± 0.57% vs. 92.70% ± 0.90%, p=4.08×10^{-4}; Rank sum test).

Electrical Receptive Fields Characterized by Linear Filter component

The linear filters of the model provided an estimate of the ERFs of each recording channel for simultaneous retinal stimulation. Figure 8(a) shows the ERF for stimuli with a net cathodic-first effect, for the most rostro-medial recording site; this channel was most responsive to stimulation of the superior-nasal retinal electrodes. The interpolated color maps depicting the linear filters at all cortical sites (n=96) from this experiment (Figure 8(b)) display a clear preference to stimulation of superior-nasal retinal electrodes for more rostral recording sites, while caudal recording sites showed a preference for stimulation of electrodes located towards the inferior retina. The gradual movement of the ERFs between these two extremes indicates topographic mapping, and is likely to be retinotopic. Using these ERFs in combination with the static nonlinearities, it is possible to link regions of high activity to stimulus features. For example, the high power in the rostral (rostral direction shown in Figure 1(b)) sites in Figure 7(b) can be attributed to high stimulation amplitude on superior-nasal retinal electrodes. Figure 8(c) more clearly illustrates the rostro-caudal movement of the linear filters, where contours represent the significant linear filter weights belonging to the most rostro-medial (green) and caudo-medial (purple) recording sites (circled in Figure 8(b)). The recording sites in this example were separated by a distance of approximately 7 mm in the cortex, which corresponds to approximately 14-23° of visual angle using a cortical magnification factor of 0.3-0.5 mm/degree (Tusa et al., 1978). The peak weightings of the linear filters for these channels were separated by about 4 mm in retinal space, which subtends a visual

angle of approximately 18°, and thus corresponds well with the recording channel separation.

While significant differences did occur between the size of ERFs for stimuli with a net cathodic-first effect and those with a net anodic-first effect on a channel by channel basis when using the EP power based model (Sign test, 0.05 level of significance), these differences were not consistent across experiments. Two out of eight experiments had larger V_N filters than V_P filters; however, one experiment had significantly larger V_P filters than V_N filters. No differences occurred between MUA-based model ERF's. Similar inconsistent differences occurred when comparing the ERF size between the two model types (EP power based models: two experiments had larger V_N filters, three had larger V_P filters; MUA-based models: three experiments had larger V_N filters, three had larger V_P filters).

Predicting responses to electrical retinal stimulation

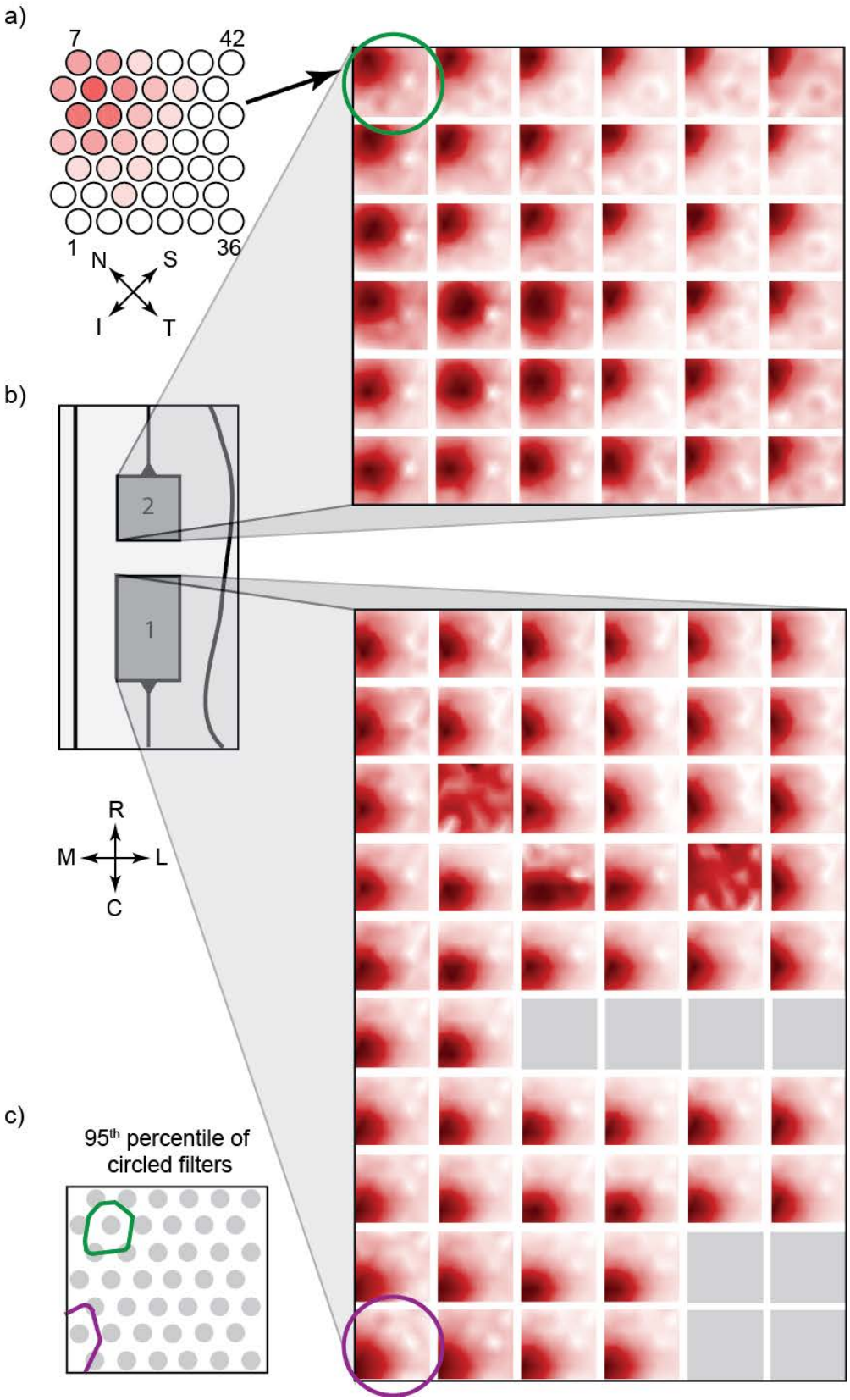

Figure 8. Linear filter maps for each recording site in one experiment. **a)** Linear filter of the most rostro-caudally located cortical site (marked with a black circle in panel b) prior to interpolation, as described in Figure 5. Only filters corresponding to anodic first stimulation (i.e. V_P) are shown. Electrode numbers correspond to those indicated in Figure 1(a). S: superior retina, I: inferior retina, N: nasal retina, T: temporal retina. **b)** Interpolated color maps representing optimized linear filters for anodic first stimulation pulses (V_P) corresponding to each of the 96 recording sites. Schematic of cortical recording areas corresponding to each of the linear filter maps is also shown. Red indicates a strong effect of a particular stimulating electrode on the activity recorded on a given cortical site. Blank sites are those that did not record a monotonically increasing response to single electrode stimulation and were thus excluded from analyses. R: rostral, C: caudal, M: medial, L: lateral. **c)** Schematic of stimulating array showing significant areas of the linear filter maps for two cortical recording sites marked with green and purple circles (corresponding to rostro-medial and caudo-medial recording sites respectively) in panel b. The shift in the electrodes that have the strongest contributions to a channels activity with cortical channel position shows that the retinotopic organization of the visual cortex is preserved with responses to simultaneous electrical stimulation of the retina.

Predicting Responses to Electrical Pattern Stimuli

To examine whether a model fitted using responses to white noise stimuli could predict responses to non-white stimuli, measured responses to oriented pattern stimuli and single electrode stimuli were compared to responses predicted by the model. Three types of patterned stimuli were used: mixed-phase, anodic-first and cathodic-first. Figure 9(a) shows the comparison between the recorded and predicted responses for the stimulus shown in Figure 2(a), where the maximum current amplitude delivered was 295μA. The responses predicted by the model corresponded well to the measured

Predicting responses to electrical retinal stimulation

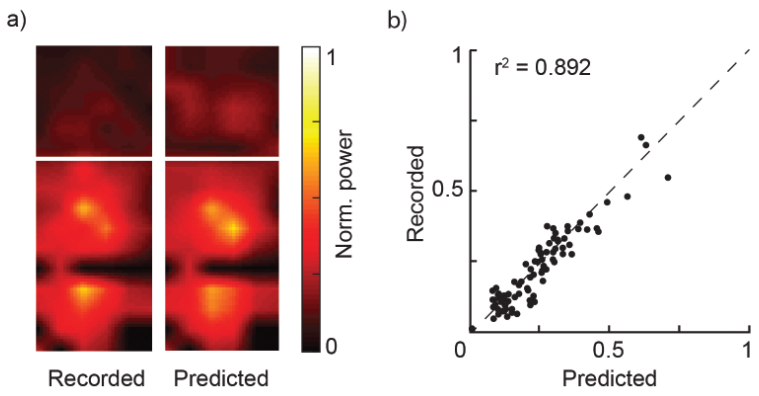

Figure 9. Recorded response and model-predicted response to the oriented pattern stimulus shown in Figure 2(a) (mixed phase first stimulus). Response is measured by the power in the EP, and shown over two recording arrays arranged as in Figure 8. The color map is normalized to the maximum recorded power. **a)** Recorded response (left), and predicted response (right). **b)** Correlation between the recorded and predicted responses (n=88 channels).

responses (Figure 9(b), r^2 = 0.89) for this stimulus.

To assess whether this effect extended to the entire set of oriented pattern stimuli, we calculated a coefficient of determination for each of the three pattern types for all experiments (Figure 10(a)). Coefficients corresponding to MUA models were significantly higher than those for EP power models for mixed-phase stimuli (MUA vs. EP power: r^2 = 0.81 ± 0.02 vs. 0.69 ± 0.03, p = 0.016; Rank sum test). There was no difference between the MUA model and EP power model for the other two stimulus types (MUA vs. EP power with anodic-first pulses: r^2 = 0.65 ± 0.07 vs. 0.65 ± 0.05, p = 0.558. MUA vs. EP power with cathodic-first pulses: 0.73 ± 0.06 vs. 0.73 ± 0.04, p = 0.457). However, for the mixed-phase and cathodic-first stimulus types, the slopes of the lines of best fit for the models fitted to MUA were significantly lower than those fitted to EP power (Figure 10(b), MUA vs. EP power with mixed-phase pulses: 0.76 ± 0.05 vs. 0.96 ± 0.09, p = 0.02.

Predicting responses to electrical retinal stimulation

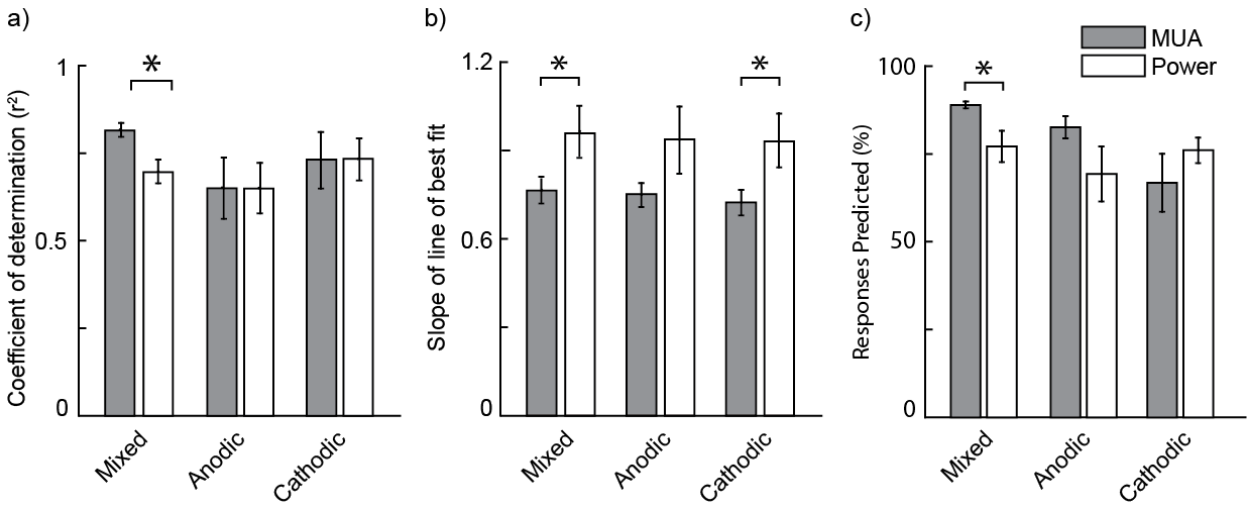

Figure 10. Comparison of the ability to predict responses to grating pattern stimuli between a spiking-based model (grey) and power-based model (white), averaged over all experiments and stimulation amplitudes (mean ±SEM) (n=40). Asterisks represent a significant difference ($p<0.05$; Rank sum test). **a)** Coefficient of determination between the model-predicted responses to oriented pattern stimuli and the recorded responses. **b)** Slope of the line of best fit for the correlation described in panel **a**. **c)** Percentage of responses to oriented pattern stimuli that were able to be predicted significantly using bootstrapping analyses.

MUA vs. EP power with anodic-first pulses: 0.75 ± 0.04 vs. 0.94 ± 0.12, $p = 0.08$. MUA vs. EP power with cathodic-first pulses: 0.72 ± 0.05 vs. 0.93 ± 0.10, $p = 0.03$; Rank sum test).

While the percentage of responses that were able to be predicted significantly above chance was generally high for both types of models and all types of stimuli (via bootstrap analysis, Figure 10(c)), the model fitted to MUA was able to predict a significantly higher number of responses for both mixed-phase and anodic-first stimuli compared to the EP power model (MUA vs. EP power with mixed-phase pulses: 94% ± 2.1% vs. 77% ± 5.2%, $p = 0.0024$. MUA vs. EP power with anodic-first pulses: 85% ± 5.4% vs. 70% ± 7.0%, $p = 0.129$. MUA vs. EP power with cathodic-first pulses: 70% ±

5.8% vs. 77% ± 6.1%, p = 0.326; Rank sum test).

When predicting responses to single electrode stimulation, coefficients of determination corresponding to EP power models were significantly higher than those corresponding to MUA models. However, both were lower than those for multi-electrode stimulation (MUA vs. EP power: r^2 = 0.26 ± 0.02 vs. 0.37 ± 0.02, p = 0.016; Rank sum test). Despite being low, the majority of both MUA and EP responses to stimuli above threshold had r^2 values significantly higher than those of the corresponding bootstrapped distributions (MUA vs. EP power: 90.6% ± 1.20% vs 92.76% ± 0.75%, averaged over above-threshold stimulus amplitudes and experiments). The slopes of the lines of best fit for the models fitted to MUA were significantly greater than those fitted to EP power (MUA vs. EP power: 0.40 ± 0.03 vs. 0.12 ± 0.01, $p << 0.001$; Rank sum test). The percentages of responses able to be predicted accurately by either model were also relatively low, and not significantly different between the model types (MUA vs. EP power: 53% ± 3.0% vs. 45% ± 1.5%, p = 0.208; Rank sum test).

Discussion

We have demonstrated that cortical responses to simultaneous stimulation of the retina are repeatable and can be predicted by a simple linear-nonlinear (LN) model. We have shown that the model can be optimized using either multi-unit activity (MUA) or power in the multi-peaked evoked potential (EP), and can be used to predict responses to types of stimulation that were not used to fit it. The optimized model also provides information about electrical receptive fields, including the relative effects of each stimulating electrode on every recording site. These ERFs show that the topographic mapping of cortical responses to single electrode stimulation (Elfar et al., 2009; Shivdasani et al., 2012; Wong et al., 2016) is maintained for simultaneous stimulation.

Comparison with Previous Studies

Studies have shown that simultaneous multi-electrode stimulation can extend the range of cortical responses possible from retinal implants beyond what is available with interleaved single electrode stimulation (Cicione et al., 2012; Matteucci et al., 2013; Dumm et al., 2014). These studies have characterized the responses of neurons to particular forms of simultaneous stimulation; however these observations cannot be generalized to patterns for which the system has not been exposed. Response models recovered by white noise electrical stimulation go some way towards solving this issue, since white noise covers a wide range of possible inputs (Chichilnisky, 2001).

In terms of visual prostheses, these investigations have been limited to *in vitro* preparations (Jepson et al., 2014; Maturana et al., 2016). Jepson et al. (2014) showed that a piecewise linear model could predict the activation of a target cell in the retina,

however the method was limited to stimulation of small numbers of electrodes at fixed stimulation amplitudes. Maturana et al. (2016) successfully showed that a LN model, mathematically similar to our model, captured the responses of RGCs to simultaneous white noise stimulation of 20 electrodes. While the success of these models aligns with that of our LN model, several important distinctions should be made. In the present study, we have demonstrated successful prediction of activity at multiple concurrent sites in the visual cortex (up to 120 recording channels) in response to stimulation, as opposed to one or two cells at a time (Maturana et al. and Jepson et al. respectively). Additionally, neither study investigated whether the suggested model performed equally well for stimulation that was non-white, as was shown for our model. Also, activation of the visual cortex more closely approximates perception elicited by electrical stimulation of the human retina than activity recorded *in vitro* (von der Heydt and Peterhans, 1989; Gilbert and Wiesel, 1990; Salzman et al., 1990; Knierim et al., 1992; van Wezel et al., 1997), and finally we made use of the same clinical grade electrode array for stimulation as has been trailed in patients (Ayton et al., 2014; Shivdasani et al., 2014).

Comparison of MUA-based and EP power-based models

Two activity measures in the visual cortex were used to fit separate LN models: MUA and EP power. These activity measures correspond to two different types of cortical processing: MUA reflects the spiking activity of multiple neurons within a radius of 150-300μm from the electrode tip (Gray et al., 1995; Henze et al., 2000); the EP contains both supra-threshold and sub-threshold components, the latter of which extends out over a larger area (Fregnac et al., 1996). The electrically evoked potentials

seen in our study were found to be in a relatively high frequency band compared to traditional local field potentials, and they exhibited a characteristic, positive-going, multi-peaked shape. A number of studies have investigated the origins of these evoked potentials and the factor that influence them (Chang, 1950; Malis and Kruger, 1956; Schoolman and Evarts, 1959; Doty and Grimm, 1962; Burke et al., 1985; Mitzdorf, 1985). Burke et al. (1985) suggested that the first two peaks of this multi-peaked response are due to conduction from Y and X type retinal ganglion cells, respectively (Enroth-Cugell and Robson, 1966; Stone, 1983). Mitzdorf (1985) found that the polarity of the peaks was dependent on the cortical depth of their recording electrode. Thus, the constant polarity of the peaks in our study may be attributed to the fact that all recording electrodes on the penetrating array were the same length (1 mm) and were thus likely to be recording from the same cortical layer. More recently, the EP has been shown to be a viable alternative to MUA when comparing percepts from visual prostheses to those from light stimulation, since a similar EP is present in photic stimulation, albeit with delayed peak latencies due to retinal processing (Nakauchi et al., 2005; Sun et al., 2011). Our findings expand on this, to show that both measures of activity can be the basis of a model for characterizing cortical responses to simultaneous stimulation of the retina. Both model types were able to predict the vast majority of white noise stimuli that were presented in all experiments. In addition, both models displayed high correlation coefficients between recorded and predicted cortical responses to retinal stimuli that were not white, and were able to predict the majority of responses to these stimuli. No consistent differences were found between different receptive field sizes. However, given that we have recorded multi-unit activity as opposed to activity from single

neurons, it is difficult to make any conclusions regarding the significance of this finding.

Some differences were present between the models however; the MUA model performed significantly better than the EP power model at predicting responses to white noise, mixed-phase first stimuli and anodic-phase first stimuli. This may be due to a greater signal to noise ratio for the MUA responses than EP power, which suggests that, for a model based on EP power, the number of repetitions for each stimulus should be increased.

Neither model performed well in predicting responses to single electrode stimulation. This may be attributed to the lower thresholds observed when stimulating across several electrodes simultaneously (Shivdasani et al., 2012), such as during white-noise stimulation, causing the model to underestimate the current required to match responses to single electrode stimulation. However, both models could predict responses to above-threshold single electrode stimulation better than chance, suggesting that the retinotopic organization is preserved. From a clinical stand-point it is therefore possible that if the highest safe amplitude of single electrode stimulation is unable to elicit a percept, simultaneous stimulation of nearby electrodes could elicit a response in the required area.

During the present study, recording channels were only considered for analyses if they exhibited a monotonic increase in response with increasing stimulation current on any single retinal electrode. As a result, a significantly greater number of sites were excluded from the MUA analyses than from EP power analyses. This likely reflects the requirement that, for recording MUA, the recording site be in close proximity to spiking cells, whereas estimating EP power does not require direct proximity to cells to register

an increase. Thus, while the MUA model predicted cortical responses more accurately than the EP power model, the latter had the advantage of characterizing a greater number of recording channels. This suggests that the activity measure on which to train the model could be altered dependent on the requirements of the application, and time available to record responses.

Clinically, the EP power would be a more attractive cortical measure as currently it is possible to record these EPs with less invasive methods than those required to record MUA; i.e., penetrating electrodes for MUA vs. scalp electrodes. Additionally, EPs have been shown to be more robust for the long term, retaining information even when spikes are lost on the same electrode (Flint et al., 2012). Thus, the EP power is an attractive measure for use with human patients, since it would eliminate the need for a further, invasive procedure, and remain informative in the long term.

Considerations for Future Applications

The model described in this study is purely spatial in nature owing to the sparse timing used between stimulus pulses. A similar model has been employed previously to model the spatio-temporal dynamics of neurons responding to visual stimulation of the retina (DeAngelis et al., 1993). We expect that by modifying our model to include a temporal dimension in our linear filters, as by Chichilnisky (2001) and Kameneva et al. (2015), the model could be extended to predict temporal dynamics of cortical responses during repetitive, high-rate stimulation, such as perceptual fading. While there is strong evidence suggesting that perceptual fading could be attributed to desensitization observed in retinal ganglion cells (Freeman and Fried, 2011), it could also be attributed

to neural mechanisms within central visual structures. Since in human trials, pulse rates for a suprachoroidal prosthesis have ranged between 50 and 500 pulses per second (pps) (Ayton et al., 2014; Shivdasani et al., 2014) and in other neural systems stimulation rates may be even higher (e.g., stimulation at up to 2000 pps has been studied in cochlear implants (Galvin III and Fu, 2005)), further investigation of the characteristics of adaptation would be of particular interest. However, in pursuit of this goal, one would have to overcome the hurdle of the stimulation artefact present in the recordings. Our stimulus pulses were 1 ms per phase and biphasic, evoking cortical responses lasting approximately 20 ms. The use of stimulus rates higher than 50 pps would not allow analysis of activity with each pulse in the stimulus train without contamination by the stimulus artifact of subsequent stimulus pulses. However, evidence suggests that desensitization of retinal ganglion cells and perceptual fading can also occur at rates lower than 50 pps (Freeman and Fried, 2011; Fornos et al., 2012). At such rates, it would be possible to remove artefacts with the same technique that we have used (Heffer and Fallon, 2008) and analyze the responses between pulses. The model we propose could then be adjusted to incorporate spatiotemporal ERFs (Chichilnisky, 2001).

Our model also provides an intriguing option for investigation of the effect of photoreceptor degeneration on responses to electrical retinal stimulation. Photoreceptor degeneration in a rat model has been shown to be accompanied by an increased activation threshold to electrical stimulation (Suzuki et al., 2004; O'Hearn et al., 2006) as well as an increase in baseline spiking (Pu et al., 2006; Stasheff, 2008). This may be a contributing factor to the inconsistencies found in the clinical results of simultaneous stimulation. Photoreceptor degeneration also leads to retinal remodeling (Jones et al.,

2003; Marc et al., 2003). Thus, it is likely that the electrical receptive fields of cortical neurons would be different in appearance to those described here.

Another factor that should be considered in future applications of this method is the effect of anesthesia on cortical activity. Given that anesthesia has been found to reduce the signal-to-noise ratio of visual responses in the cat visual cortex (Livingstone and Hubel, 1981) and preserve the main tuning characteristics of V1 neurons in monkeys (Lamme et al., 1998) and mice (Niell and Stryker, 2010), we expect that the responses to electrical stimulation in an awake cat would be stronger but have similar tuning properties and, therefore, be well suited for application of this method.

The model we have presented provides novel insights into the effects of interactions between electrodes during simultaneous electrical retinal stimulation. It is expected that with some adjustments, this model could provide a potential approach for choosing optimal stimulation patterns for eliciting specific neural activity (for example, activity more akin to that elicited by visual stimulation). This would entail first fitting the model to responses of the system in question to spatial white noise stimulation. Then, a second optimization algorithm would be used to compute stimulation patterns that would be likely to produce a desired cortical response. In this way, the model could be used to ultimately increase the resolution of the implant.

Conclusion

In this study, we have shown that cortical responses to simultaneous stimulation of the retina are consistent and repeatable. We investigated the effects of electrode interactions of retinal stimulation by creating a linear-nonlinear model of visual cortex

responses. We showed that the model could accurately predict spiking neural responses to both white-noise stimulation and patterned stimulation. The model could also be based on an alternative measure of cortical activity, namely power in the evoked potentials, suggesting that, for clinical applications, a less invasive measure could be applicable. The model we describe provides an effective means of understanding the spatial interactions of retinal stimulation at the level of the cortex, showing that they are predominantly linear and the electrical receptive fields of cortical recording channels are topographically organized. The predictive success of our model shows promise for efficiently determining optimal stimulation paradigms for shaping neural activity with a neural prosthesis.

Acknowledgements

The authors thank Penny Allen, Jonathan Yeoh, and Chi Luu for surgeries; Carla Abbott, Alice Brandli, Alexia Saunders, Michelle McPhedran, Alison Neil, Dimitra Stathopoulos, Stephanie Epp, and Ceara McGowan for experimental assistance and animal handling; Owen Burns and Vanessa Maxim for manufacturing of the electrodes; and Thomas Spencer, Faith Lamont, Ali Almasi, Felix Aplin, Rosemary Cicione, and Ronald Leung for assistance with data collection. This research was supported by the Australian Research Council through its Special Research Initiative in Bionic Vision Science and Technology awarded to Bionic Vision Australia, the Bertalli Family Foundation to the Bionics Institute, and a project grant from the National Health and Medical Research Council, Australia (GNT#1063093). The Bionics Institute acknowledges the support it receives from the Victorian Government through its Operational Infrastructure Program. KJH was

supported by an Australian Postgraduate Award through the Australian Government, and a postgraduate scholarship from the National Information and Communication Technology Australia (NICTA - www.nicta.com.au/). NICTA is funded by the Australian Government as represented by the Department of Broadband, Communications and the Digital Economy (www.communications.gov.au/) and the Australian Research Council through the ICT Centre of Excellence program. ANB and YTW acknowledge support under the Australian Research Council's Discovery Projects funding scheme (Project DP140104533).

References

Auner GW, You R, Siy P, McAllister JP, Talukder M, Abrams GW (2008) Development of a Wireless High-Frequency Microarray Implant for Retinal Stimulation. Artificial Sight 2008:169-186.

Ayton LN, Blamey PJ, Guymer RH, Luu CD, Nayagam DA, Sinclair NC, Shivdasani MN, Yeoh J, McCombe MF, Briggs RJ, others (2014) First-in-human trial of a novel suprachoroidal retinal prosthesis. PloS one 9:e115239.

Barry MP, Dagnelie G, Group AIS (2012) Use of the Argus II retinal prosthesis to improve visual guidance of fine hand movements. Investigative Ophthalmology & Visual Science 53:5095.

Benjamini Y, Hochberg Y (1995) Controlling the false discovery rate: a practical and powerful approach to multiple testing. Journal of the Royal Statistical Society Series B (Methodological):289-300.

Boinagrov D, Pangratz-Fuehrer S, Goetz G, Palanker D (2014) Selectivity of direct and network-mediated stimulation of the retinal ganglion cells with epi-, sub-and intraretinal electrodes. Journal of neural engineering 11:026008.

Burke W, Burne J, Martin P (1985) Selective block of Y optic nerve fibres in the cat and the occurrence of inhibition in the lateral geniculate nucleus. The Journal of Physiology 364:81-92.

Chang H-T (1950) The repetitive discharges of corticothalamic reverberating circuit. Journal of Neurophysiology.

Chichilnisky E (2001) A simple white noise analysis of neuronal light responses. Network: Computation in Neural Systems 12:199-213.

Cicione R, Shivdasani MN, Fallon JB, Luu CD, Allen PJ, Rathbone GD, Shepherd RK, Williams CE (2012) Visual cortex responses to suprachoroidal electrical stimulation of the retina: Effects of electrode return configuration. Journal of Neural Engineering 9:036009.

da Cruz L, Coley BF, Dorn J, Merlini F, Filley E, Christopher P, Chen FK, Wuyyuru V, Sahel J,

Stanga P (2013) The Argus II epiretinal prosthesis system allows letter and word reading and long-term function in patients with profound vision loss. British Journal of Ophthalmology 0:1-5.

DeAngelis GC, Ohzawa I, Freeman R (1993) Spatiotemporal organization of simple-cell receptive fields in the cat's striate cortex. II. Linearity of temporal and spatial summation. Journal of Neurophysiology 69:1118-1135.

Doty RW, Grimm FR (1962) Cortical responses to local electrical stimulation of retina. Experimental Neurology 5:319-334.

Dumm G, Fallon J, Williams C, Shivdasani M (2014) Virtual electrodes by current steering in retinal prostheses. Investigative Ophthalmology & Visual Science 55:8077–8085.

Elfar SD, Cottaris NP, Iezzi R, Abrams GW (2009) A cortical (V1) neurophysiological recording model for assessing the efficacy of retinal visual prostheses. Journal of Neuroscience Methods 180:195-207.

Enroth-Cugell C, Robson JG (1966) The contrast sensitivity of retinal ganglion cells of the cat. The Journal of Physiology 187:517-552.

Flint RD, Lindberg EW, Jordan LR, Miller LE, Slutzky MW (2012) Accurate decoding of reaching movements from field potentials in the absence of spikes. Journal of neural engineering 9:046006.

Fornos AP, Sommerhalder J, da Cruz L, Sahel JA, Mohand-Said S, Hafezi F, Pelizzone M (2012) Temporal Properties of Visual Perception on Electrical Stimulation of the RetinaPerception upon Electrical Stimulation of the Retina. Investigative ophthalmology & visual science 53:2720-2731.

Freeman DK, Fried SI (2011) Multiple components of ganglion cell desensitization in response to prosthetic stimulation. Journal of neural engineering 8:016008.

Fregnac Y, Bringuier V, Chavane F (1996) Synaptic integration fields and associative plasticity of visual cortical cells in vivo. Journal of Physiology-Paris 90:367-372.

Galvin III JJ, Fu Q-J (2005) Effects of stimulation rate, mode and level on modulation detection by cochlear implant users. Journal of the Association for Research in Otolaryngology 6:269-279.

Gilbert CD, Wiesel TN (1990) The influence of contextual stimuli on the orientation selectivity of cells in primary visual cortex of the cat. Vision Research 30:1689-1701.

Gray CM, Maldonado PE, Wilson M, McNaughton B (1995) Tetrodes markedly improve the reliability and yield of multiple single-unit isolation from multi-unit recordings in cat striate cortex. Journal of Neuroscience Methods 63:43-54.

Habib AG, Cameron MA, Suaning GJ, Lovell NH, Morley JW (2013) Spatially restricted electrical activation of retinal ganglion cells in the rabbit retina by hexapolar electrode return configuration. Journal of Neural Engineering 10:036013.

Heffer LF, Fallon JB (2008) A novel stimulus artifact removal technique for high-rate electrical stimulation. Journal of Neuroscience Methods 170:277-284.

Henze DA, Borhegyi Z, Csicsvari J, Mamiya A, Harris KD, Buzsáki G (2000) Intracellular features predicted by extracellular recordings in the hippocampus in vivo. Journal of Neurophysiology 84:390-400.

Horsager A, Greenberg RJ, Fine I (2010) Spatiotemporal interactions in retinal prosthesis subjects. Investigative Ophthalmology & Visual Science 51:1223-1233.

Predicting responses to electrical retinal stimulation

Humayun MS, de Juan Jr E, Weiland JD, Dagnelie G, Katona S, Greenberg RJ, Suzuki S (1999) Pattern electrical stimulation of the human retina. Vision Research 39:2569-2576.

Jensen RJ, Rizzo JF (2006) Thresholds for activation of rabbit retinal ganglion cells with a subretinal electrode. Experimental eye research 83:367-373.

Jepson L, Hottowy P, Gunning D, Mathieson K, Dabrowski W, Litke A, Chichilnisky E (2014) Spatially Patterned Electrical Stimulation to Enhance Resolution of Retinal Prostheses. The Journal of Neuroscience 34:4871-4881.

Jones BW, Watt CB, Frederick JM, Baehr W, Chen CK, Levine EM, Milam AH, Lavail MM, Marc RE (2003) Retinal remodeling triggered by photoreceptor degenerations. Journal of Comparative Neurology 464:1-16.

Kameneva T, Abramian M, Zarelli D, Něsić D, Burkitt AN, Meffin H, Grayden DB (2015) Spike history neural response model. Journal of computational neuroscience 38:463-481.

Knierim JJ, Van Essen DC, others (1992) Neuronal responses to static texture patterns in area V1 of the alert macaque monkey. Journal of Neurophysiology 67:961-980.

Kotecha A, Zhong J, Stewart D, da Cruz L (2014) The Argus II prosthesis facilitates reaching and grasping tasks: a case series. BMC Ophthalmology 14:71.

Lamme VA, Zipser K, Spekreijse H (1998) Figure-ground activity in primary visual cortex is suppressed by anesthesia. Proceedings of the National Academy of Sciences 95:3263-3268.

Livingstone MS, Hubel DH (1981) Effects of sleep and arousal on the processing of visual information in the cat. Nature 291:554-561.

Malis LI, Kruger L (1956) Multiple response and excitability of cat's visual cortex. Journal of Neurophysiology 19:172-186.

Marc RE, Jones BW, Watt CB, Strettoi E (2003) Neural Remodeling in Retinal Degeneration. Progress in Retinal and Eye Research 22:607-655.

Matteucci PB, Chen SC, Tsai D, Dodds CWD, Dokos S, Morley JW, Lovell NH, Suaning GJ (2013) Current Steering in Retinal Stimulation via a Quasimonopolar Stimulation Paradigm. Investigative Opthalmology & Visual Science 54:4307-4320.

Maturana MI, Apollo NV, Hadjinicolaou AE, Garrett DJ, Cloherty SL, Kameneva T, Grayden DB, Ibbotson MR, Meffin H (2016) A Simple and Accurate Model to Predict Responses to Multi-electrode Stimulation in the Retina. PLOS Comput Biol 12:e1004849.

Mitra PP, Pesaran B (1999) Analysis of dynamic brain imaging data. Biophysical Journal 76:691-708.

Mitzdorf U (1985) Current source-density method and application in cat cerebral cortex: investigation of evoked potentials and EEG phenomena. Physiological Reviews 65:37-100.

Nakauchi K, Fujikado T, Kanda H, Morimoto T, Choi JS, Ikuno Y, Sakaguchi H, Kamei M, Ohji M, Yagi T (2005) Transretinal electrical stimulation by an intrascleral multichannel electrode array in rabbit eyes. Graefe's Archive for Clinical and Experimental Ophthalmology 243:169-174.

Niell CM, Stryker MP (2010) Modulation of visual responses by behavioral state in mouse visual cortex. Neuron 65:472-479.

O'Hearn TM, Sadda SR, Weiland JD, Maia M, Margalit E, Humayun MS (2006) Electrical stimulation in normal and retinal degeneration (rd1) isolated mouse retina. Vision

Research 46:3198-3204.

Pillow JW, Paninski L, Uzzell VJ, Simoncelli EP, Chichilnisky E (2005) Prediction and decoding of retinal ganglion cell responses with a probabilistic spiking model. The Journal of Neuroscience 25:11003-11013.

Pu M, Xu L, Zhang H (2006) Visual response properties of retinal ganglion cells in the royal college of surgeons dystrophic rat. Investigative Ophthalmology & Visual Science 47:3579-3585.

Rizzo JF, Wyatt J, Loewenstein J, Kelly S, Shire D (2003) Perceptual Efficacy of Electrical Stimulation of Human Retina with a Microelectrode Array during Short-Term Surgical Trials. Investigative Ophthalmology & Visual Science 44:5362-5369.

Salzman CD, Britten KH, Newsome WT (1990) Cortical microstimulation influences perceptual judgements of motion direction. Nature 346:174-177.

Schoolman A, Evarts EV (1959) Responses to lateral geniculate radiation stimulation in cats with implanted electrodes. Journal of Neurophysiology 22:112-129.

Schwartz G, Rieke F (2011) Nonlinear spatial encoding by retinal ganglion cells: when 1+ 1 $\neq$ 2. The Journal of General Physiology 138:283-290.

Shivdasani MN, Fallon JB, Luu CD, Cicione R, Allen PJ, Morley JW, Williams CE (2012) Visual Cortex Responses to Single-and Simultaneous Multiple-Electrode Stimulation of the Retina: Implications for Retinal Prostheses. Investigative Ophthalmology & Visual Science 53:6291-6300.

Shivdasani MN, Sinclair NC, Dimitrov PN, Varsamidis M, Ayton LN, Luu CD, Perera T, McDermott HJ, Blamey PJ (2014) Factors Affecting Perceptual Thresholds in a Suprachoroidal Retinal ProsthesisFactors Affecting Retinal Prosthesis Thresholds. Investigative ophthalmology & visual science 55:6467-6481.

Stasheff SF (2008) Emergence of sustained spontaneous hyperactivity and temporary preservation of OFF responses in ganglion cells of the retinal degeneration (rd1) mouse. Journal of Neurophysiology 99:1408-1421.

Stingl K, Bartz-Schmidt KU, Besch D, Braun A, Bruckmann A, Gekeler F, Greppmaier U, Hipp S, Hörtdörfer G, Kernstock C (2013) Artificial vision with wirelessly powered subretinal electronic implant alpha-IMS. Proceedings of the Royal Society of London B: Biological Sciences 280:20130077.

Stingl K, Bartz-Schmidt KU, Besch D, Chee CK, Cottriall CL, Gekeler F, Groppe M, Jackson TL, MacLaren RE, Koitschev A (2015) Subretinal Visual Implant Alpha IMS–Clinical trial interim report. Vision research 111:149-160.

Stone J (1983) On the Understanding of Visual Processing in the Diencephalon. In: Parallel Processing in the Visual System, pp 149-193: Springer.

Sun J, Lu Y, Cao P, Li X, Cai C, Chai X, Ren Q, Li L (2011) Spatiotemporal properties of multipeaked electrically evoked potentials elicited by penetrative optic nerve stimulation in rabbits. Investigative Ophthalmology & Visual Science 52:146-154.

Suzuki S, Humayun MS, Weiland JD, Chen S-J, Margalit E, Piyathaisere DV, de Juan JE (2004) Comparison of electrical stimulation thresholds in normal and retinal degenerated mouse retina. Japanese Journal of Ophthalmology 48:345-349.

Thomson DJ (1982) Spectrum estimation and harmonic analysis. Proceedings of the IEEE 70:1055-1096.

Tusa R, Palmer L, Rosenquist A (1978) The retinotopic organization of area 17 (striate cortex) in the cat. Journal of Comparative Neurology 177:213-235.

van Wezel RJ, Lankheet MJ, Fredericksen R, Verstraten FA, van de Grind W (1997) Responses of complex cells in cat area 17 to apparent motion of random pixel arrays. Vision Research 37:839-852.

Villalobos J, Allen PJ, McCombe MF, Ulaganathan M, Zamir E, Ng DC, Shepherd RK, Williams CE (2012) Development of a surgical approach for a wide-view suprachoroidal retinal prosthesis: evaluation of implantation trauma. Graefe's Archive for Clinical and Experimental Ophthalmology 250:399-407.

von der Heydt R, Peterhans E (1989) Mechanisms of contour perception in monkey visual cortex. I. Lines of pattern discontinuity. The Journal of Neuroscience 9:1731-1748.

Wilke R, Gabel V-P, Sachs H, Schmidt K-UB, Gekeler F, Besch D, Szurman P, Stett A, Wilhelm B, Peters T (2011) Spatial resolution and perception of patterns mediated by a subretinal 16-electrode array in patients blinded by hereditary retinal dystrophies. Investigative Ophthalmology & Visual Science 52:5995-6003.

Wong YT, Halupka K, Kameneva T, Cloherty SL, Grayden DB, Burkitt AN, Meffin H, Shivdasani MN (2016) Spectral distribution of local field potential responses to electrical stimulation of the retina. Journal of neural engineering 13:036003.